Abiotic drivers of a deep cyanobacteria layer in a stratified and eutrophic lake

J. Taylor[1,2], M. Hondzo[1,2], and V. R. Voller[1,2]

[1]University of Minnesota, Twin Cities – Department of Civil, Environmental, and Geo-Engineering
[2]University of Minnesota, Twin Cities – St. Anthony Falls Laboratory

Key Points:

- In a eutrophic and stratified lake environment, magnitude of subsurface cyanobacteria peak concentration is driven primarily by thermocline depth and temperature
- In a eutrophic and stratified lake environment, center of gravity of subsurface cyanobacterial biomass is driven primarily by surface layer depth and temperature

Corresponding author: J. Taylor, tayl1562@umn.edu

Abstract

Harmful algal blooms (HABs), in particular those consisting of the cyanobacteria *Microcystis*, are becoming increasingly more common across the globe. Despite the growing body of evidence that suggests vertical heterogeneity of *Microcystis* can be a precursor to HAB formation, the abiotic drivers of vertical distribution of *Microcystis* are poorly understood in the field environment. The prediction of subsurface cyanobacteria is also pertinent because subsurface concentrations are not easily recognizable to the public or lake system managers, creating an unnoticed safety hazard. High-frequency temporal and vertical data were collected from an Eulerian research station anchored in a stratified and eutrophic lake for five months. Data show that the magnitude of the subsurface *Microcystis* concentration peak and the center of gravity of the deep cyanobacteria layer are statistically significantly mediated by the thermal structure of the lake. The peak subsurface cyanobacteria biovolume scales linearly with the thermocline depth and temperature, whereas the center of gravity of the subsurface cyanobacteria biovolume scales linearly with the mixed layer depth and temperature. Furthermore, our data suggest there is a seasonal evolution of the subsurface cyanobacteria center of gravity that could potentially indicate timing of HAB onset. Based on easily measured parameters associated with the vertical lake temperature profile and meteorological conditions, we provide evidence of predictable trends in subsurface cyanobacteria variables.

1 Introduction

Harmful algal blooms are one of the most imminent threats to freshwater quality across the globe (O'Neil et al., 2012; Huisman et al., 2018). Of the HAB-forming cyanobacteria species, *Microcystis* are of particular concern due to their ubiquity and their production of Microcystin toxins. There are numerous evolutionary advantages that allow *Microcystis* to thrive across the globe, and one such advantage in stratified lakes is the ability of vertical motility. Cell buoyancy is modulated by adjusting ballast weight through production or metabolism of dense carbohydrates to offset low density intracellular gas vesicles, *Microcystis* are able to move up or down the water column (Reynolds et al., 1987). The speed of unicellular vertical motility can be greatly enhanced by forming colonies, which is a typical occurrence in natural environments (Xiao et al., 2018).

Traditionally, *Microcystis* vertical migration in natural environments has been hypothesized to be nutrient-driven chemotaxis (Fogg & Walsby, 1971; Ganf & Oliver, 1982). However, as lakes become more eutrophic and nutrients become a less limiting substrate, abiotic factors tend to dominate *Microcystis* vertical motility (Xiao et al., 2018). Most of the work on abiotic drivers has focused on light, wind, and temperature. Thomas and Walsby (1985, 1986) demonstrated experimentally that *Microcystis* cells will increase in density under high irradiance conditions to sink to a preferred low light intensity, but their ability to regain buoyancy was dependent on water temperature. Cao et al. (2006) suggested vertical distributions of different phytoplankton species, especially *Microcystis*, were largely correlated with wind events (and had no correlation with nutrients) in a field study of Lake Taihu, China. As a result, it has been suggested the relationship between *Microcystis* vertical motility and timing of HAB onset should be explored more in depth (Xiao et al., 2018; Zhu et al., 2018; Liu et al., 2019). There have been several models formulated to simulate *Microcystis* vertical motility as a function of abiotic factors (Wallace et al., 2000; Medrano et al., 2013; Zhu et al., 2018), and Yao et al. (2017) connected their simulations of *Microcystis* motility to a hypothesis of necessary conditions for bloom formation, but none have had a long-term, high-frequency, *in situ* temporal data set for validation.

Aside from being active movers, *Micrycosystis* can also act as passive particles in a water column. Field investigations including Bormans et al. (1999) suggest surface dynamics play the largest role in determining vertical distribution of *Microcystis*. Marti et al. (2016) used relevant time scales of vertical transport in the surface layer and the metal-

imnion, vertical mixing in the surface layer and the metalimnion, and vertical migration of cyanobacteria to characterize when algae were acting as free movers or passive particles. It was suggested, through field work and 3-D simulations, that the time-scale hierarchy–how fast one process happens compared to another–determines success of particular algal species at specific locations in the lake. A field study by Hozumi et al. (2019) demonstrated that low turbulence levels in the surface layer of Lake Kinneret, Israel led to a thin, dense *Microcystis* scum layer, while higher levels of turbulence led to a thick, sparse *Microcystis* layer. These findings were corroborated in a mesocosm experiment conducted by X. Wu et al. (2019). To further complicate the relationship between lake hydrodynamics and cyanobacteria, Sommer et al. (2017) demonstrated that dense layers of motile algae can create a great enough density instability to modulate the mixed layer depth, as corroborated by the field study conducted by Sepúlveda Steiner et al. (2019).

The phenomenon of subsurface peaks in cyanobacterial biomass concentration has been studied extensively in both ocean and lake environments. This feature is often referred to as a deep chlorophyll maximum, or DCM (Cullen, 1982), and the zone in which this increase in biomass occurs is called a deep chlorophyll layer, or DCL (Brooks & Torke, 1977). The abiotic drivers of DCL formation have been extensively studied (Cullen, 2015). Huisman et al. (2006) demonstrated through numerical simulations that there exists a minimum turbulence level in the surface layer of the ocean in order to achieve a stable DCM. Scofield et al. (2017) conducted a field study on Lake Ontario and determined significant dependencies of DCM magnitude and location on the temperature profile of a lake; Sanful et al. (2017) demonstrated euphotic depth was the primary driver of DCM formation and maintenance in another field study. Somavilla et al. (2019) connected deep chlorophyll phenomena to surface blooms in an oceanic environment: field data demonstrated that cyanobacterial biomass was prevalent below the diurnal mixed layer, towards a DCL, when the net heat flux at the water surface became positive on a seasonal timescale. Lastly, despite being a major topic of study for four decades, the actual definition of a DCL or DCM is largely ambiguous. How deep is "deep"? What is the depth of the maximum biomass for profiles with two or more peaks in the DCL? Xu et al. (2019) developed a robust machine learning algorithm to help unify these definitions, but perhaps the problem is in the parameters we are defining than in how we define them.

The work highlighted above has brought many interesting insights to the field. However, as is almost always the case when dealing with microorganisms, discrepancies exist between experiments with short-term, high-frequency observations and field data with long-term, low-frequency observations. Further, DCM and DCL definitions and parameters (or lack thereof) make it difficult to draw cohesive conclusions between studies. To bridge these gaps, we anchored a research station from May to August of 2017 in a stratified and eutrophic lake with a history of *Microcystis* blooms. This research station recorded meteorological and water temperature conditions every five minutes and water quality variables every two hours. Data were then used to inform and validate a stepwise regression model to determine the relationship between the light, wind speed, and temperature profiles of a lake with the magnitude and shape of a deep cyanobacteria layer (DCL from here on out), a potential precursor to a harmful algal bloom. Formal definitions and a new shape parameter for the DCL were introduced, as well as a potential method for predicting bloom formation when a DCL is present.

2 Methods

2.1 Field site

South Center Lake, Fig. 1a, is a eutrophic and dimictic lake in Chisago County, MN that stratifies from May to October. It has a surface area of approximately 3.3 km^2, a maximum depth of 33 m, an average depth of nearly 5 m, and its shoreline is mostly developed. Due to its status as a Minnesota Pollution Control Agency (MPCA) Sentinel lake, South

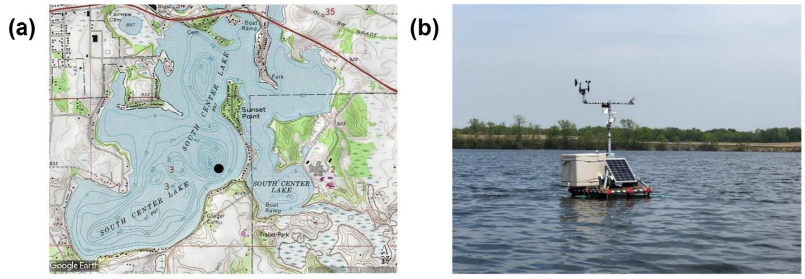

Figure 1: **(a)** USGS contour map of South Center Lake. Black dot indicates position of research station. **(b)** Research station.

Center Lake has a wealth of historical data, with the first lake survey occurring in 1942 and regular water quality data from 1997 to present day. This historical data, which indicates a reoccurring summer-time *Microcystis* bloom, was used to supplement measurements from our research station (Engel et al., 2011). For instance, historic phytoplankton assemblages indicate South Center Lake, in a location near where our measurements were taken, is almost entirely cyanobacteria dominant year-round, besides some diatoms and green algae in early summer. MPCA data were also used to corroborate grab sample measurements, detailed in Section 2.3.

2.2 Research station

The research station was anchored in South Center Lake from May 12, 2017 to October 30, 2017 (Fig. 1b). The data used in analysis extends to September 3rd, 2017–the end of *Microcystis* domination (Wilkinson et al., 2020). The lake depth was 14 m deep at the location of the water station. The research station records meteorological measurements–wind speed, wind direction, air temperature, relative humidity, photosynthetically active radiation (PAR), and rain depth–every five minutes. In addition, a thermistor chain records water temperature at depths of 0.1, 1, 2, 3, 4, 5, 6, 7, 8, 10, 12, and 14 m every five minutes. The water quality profiler takes measurements of dissolved oxygen concentration, pH, phycocyanin concentration, PAR, specific conductivity, and water temperature at depths of 1, 1.5, 2, 2.5, 3, 3.5, 4, 4.5, 5, 6, 7, 8, 9, 10, 11, 12, 13, and 14 m every two hours. For a full description of equipment used, see Wilkinson et al. (2020). An example profile for temperature, biovolume, and PAR is shown in Fig. 2.

2.3 Data analysis

Water column parameters that describe the vertical thermal structure of the lake were determined from the Lake Analyzer and Lake Heat Flux Analyzer software in Matlab (Read et al., 2011; Woolway et al., 2015). Weekly grab samples were taken to measure nutrient, phycocyanin, and estimate biovolume concentrations throughout the water column. The *in situ* field measurements of phycocyanin, a protein found only in cyanobacteria, was linearly regressed to the laboratory measurements of the corresponding phycocyanin grab samples and the *Microcystis* biovolume estimates (Wilkinson et al., 2020).

The average mode-1 vertical seiche period of South Center Lake estimated from the Lake Analyzer software was approximately four hours. Water temperature and research station data were averaged over this seiche period to determine diurnal and seasonal trends. The mixed layer depth, h_{ML}, was defined as the first depth with a temperature difference of at least -0.3^{o}C from the surface water temperature. The thermocline depth, h_T, was defined as the depth at which the maximum temperature gradient occurs. The euphotic depth, h_{EP} was defined as the depth at which PAR intensity was 1% of the PAR intensity of the

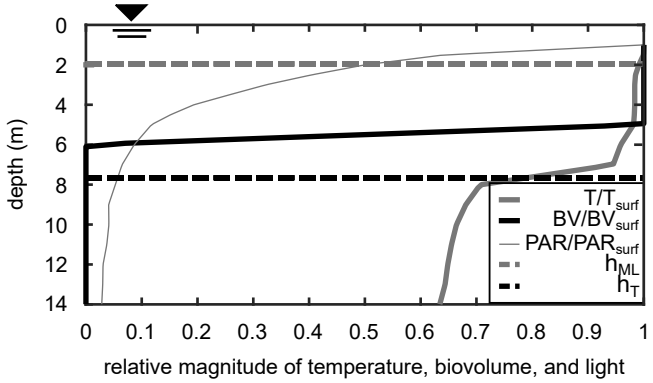

Figure 2: Profile from 24 May, 2017 6:02pm of normalized temperature (thick solid gray line), biovolume (thick solid black line), and light (thin solid gray line) profile generated from research station profiler data. Mixed layer depth (horizontal dashed gray line) and thermocline depth (horizontal dashed black line) also shown. Water surface is at 0 m, and the lake bed is at 14 m. Here, $\mathrm{T}_{surf} = 14.77^{o}\mathrm{C}$, $\mathrm{BV}_{surf} = 2.76{\times}10^{6}$ $\mu\mathrm{m}^3/\mathrm{mL}$, and PAR_{surf} = 166.3 $\mu\mathrm{mol/s/m}^2$.

water surface. Mixed layer temperature, T_{ML}, was then defined as the water temperature at the mixed layer depth, with corresponding definitions for the thermocline temperature, T_{T}, and the euphotic temperature, T_{EP}. The thermocline steepness, m_{T}, was defined as the temperature gradient at the thermocline. Since research station data were recorded at discrete depths (Sec. 2.2), a piecewise linearly interpolated line was fitted to research station profiler data to create pseudo-continuous profiles. For the convenience of the reader, key parameters derived from measurements along with appropriate scalings are given in Table 1.

Table 1: Relevant temperature profile parameters[a]

parameter	**variable**	**comment**
mixed layer depth	$\tilde{h}_{ML}$	depth of base of surfaced mixed layer
thermocline depth	$\tilde{h}_{T}$	depth of maximum magnitude temperature gradient
euphotic dpeth	$\tilde{h}_{EP}$	depth where PAR reaches 1% of surface PAR
mixed layer temperature	$\tilde{T}_{ML}$	water temperature at mixed layer depth
thermocline temperature	$\tilde{T}_{T}$	water temperature at thermocline depth
euphotic temperature	$\tilde{T}_{EP}$	water temperature at euphotic depth
thermocline steepness	$\tilde{m}_{T}$	temperature gradient at the thermocline depth

[a] Parameters have been made dimensionless, as indicated by the tilde. All depths were normalized by dividing by h_{max} = 14m, the maximum depth of the water column at the location of the research station. All temperature were normalized by multiplying by α, the coefficient of thermal expansion (^{o}C). The thermocline steepness was normalized by multiplying by $\alpha\mathrm{h}_{max}$.

2.4 Deep cyanobacteria layer definitions

A deep cyanobacteria layer (DCL) is defined to be present if there exists a biovolume concentration, C, below the diurnal mixed layer depth that is greater than the maximum concentration within the diurnal mixed layer (Fig. 3). If this condition is met, then the top of the DCL, z_{TOP}, is defined as the first depth of increasing phycocyanin concentration below the mixed layer. The bottom of the DCL, z_{BOT}, is defined as the first depth after z_{TOP} such that the phycocyanin concentration goes below the average concentration within the mixed layer. The dimensionless center of gravity of the DCL, z_{CG}, can then be defined as

$$z_{CG} = \frac{1}{h_{max}} \left(\frac{\int_{z_{BOT}}^{z_{TOP}} zCdz}{\int_{z_{BOT}}^{z_{TOP}} Cdz} \right) \tag{1}$$

where h_{max} is the maximum depth of the water column at the location of the research station (h_{max} = 14m). Dividing by h_{max} ensures not only that z_{CG} is dimensionless, but also that it is scaled from 0 to 1, from the water surface to the lake bed, respectively (Fig. 4).

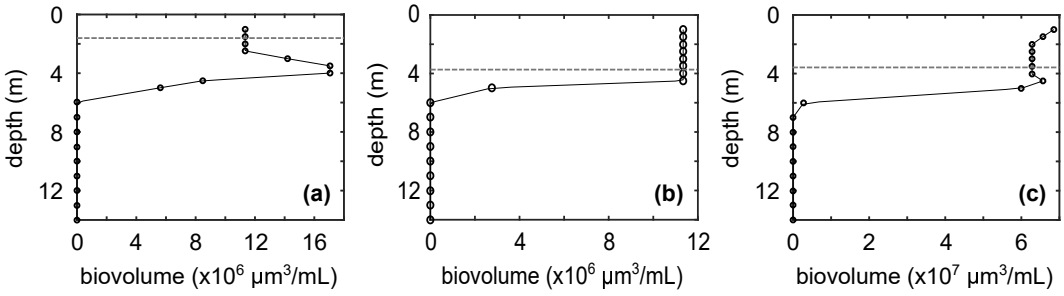

Figure 3: Example biovolume profiles when **(a)** a DCL is present (July 4th, 2017 18:00), **(b)** a uniform biovolume distribution with no DCL present (July 13th, 2017 04:00), and **(c)** a surface biovolume peak with no DCL present (August 4th, 2017 16:00). Thin black lines with open circle markers indicate the biovolume profile, and horizontal dashed grey lines indicate the mixed layer depth. Note that in **(c)**, although there is an increase in biovolume below the mixed layer depth, it is not significantly large enough compared to the average concentration within the mixed layer to be considered a DCL.

C_{DCL} is a dimensionless variable that describes the relative magnitude of the DCL peak biovolume concentration to the biovolume concentration within the mixed layer and is defined as follows:

$$C_{DCL} = \frac{C_{DCL,max} - C_{ML,avg}}{C_{ML,avg}} \tag{2}$$

where $C_{DCL,max}$ is the maximum biovolume concentration within the DCL and $C_{ML,avg}$ is the average biovolume concentration in the mixed layer.

2.5 Modeling DCL variables

We can ensure DCL definitions are physically meaningful if we can predict them with relevant forcings. Under low nitrogen to phosphorus ratio conditions, which is preferred by *Microcystis* (Fujimoto et al., 1997; Wurtsbaugh et al., 2019), it is hypothesized that the characteristics of the DCL are controlled by the vertical temperature structure and light conditions in the lake. That is, if a DCL is present, its center of gravity and magnitude can be expressed as functions of the variables in Table 1 to arrive at the following:

$$z_{CG} = f(\tilde{h}_{ML}, \tilde{h}_T, \tilde{h}_{EP}, \tilde{T}_{ML}, \tilde{T}_T, \tilde{T}_{EP}, \tilde{m}_T) \tag{3}$$

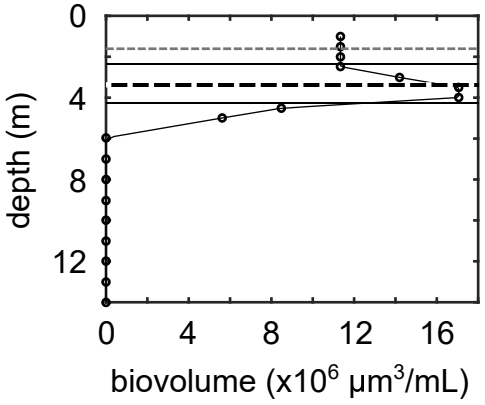

Figure 4: Example biovolume profile with a DCL (July 4th, 2017 18:00, Fig. 3a). Thin black line with open circle markers indicate the biovolume profile, horizontal dashed gray line indicated the mixed layer depth, horizontal solid black lines indicate the bounds of the DCL, and horizontal dashed black line indicates the DCL center of gravity.

$$C_{DCL} = g(\tilde{h}_{ML}, \tilde{h}_T, \tilde{h}_{EP}, \tilde{T}_{ML}, \tilde{T}_T, \tilde{T}_{EP}, \tilde{m}_T) \tag{4}$$

A regression analysis was performed to determine what physical parameters and interactions of physical parameters had the most significant impact on the normalized maximum biovolume concentration in the DCL, C_{DCL}, and the normalized center of gravity of biovolume in the DCL, z_{CG}. Matlab's Statistical and Machine Learning Toolbox and, in particular, the Matlab function stepwiselm was used. Daytime profiles were separated from nighttime profiles to determine the impact of the light regime on the DCL characteristics. In the analysis of the nighttime profiles, variables $\tilde{T}_{EP}$ and $\tilde{h}_{EP}$ were dropped. A model that includes both linear and bi-linear (interaction) terms was then generated to predict $C_{DCL,all}$, $C_{DCL,day}$, $C_{DCL,night}$, $z_{CG,all}$, $z_{CG,day}$, and $z_{CG,night}$. Once full models had been derived, observational trends were used to create parsimonious models with the lowest number of parameters that were still able to explain the data variability with statistical significance.

3 Results

3.1 Seasonal trends of water temperature, biological, and meteorological data

The temperature and biovolume profiles depicted seasonal and vertical patterns of thermal stratification and cyanobacterial accrual from June to October 2017 (Fig. 5). Temperature stratification over the lake depth was established before June 2017 and the lake experienced thermal structure overturn shortly before November. Significant subsurface peaks in biovolume appeared at the beginning of June and July, and a surface bloom formed in early August. Grab samples show *Microcystis* was the dominant biovolume genera up until the surface bloom in early August when *Planktothrix* began to dominate the composition of cyanobacteria (Wilkinson et al., 2020). For the remainder of the analysis, we will focus only on the period of stratification from June to October, with a particular emphasis from June until the harmful algal bloom in early August when *Microcystis* was dominant.

Time series of wind speed and air-water temperature difference are included to provide a sense of the meteorological forcings of the thermal and algal structure of the lake (Fig. 6). Overall, surface water temperatures were higher than the air temperatures, thereby indicating prevalence of natural cooling due to the heat loss from the surface mixed layer

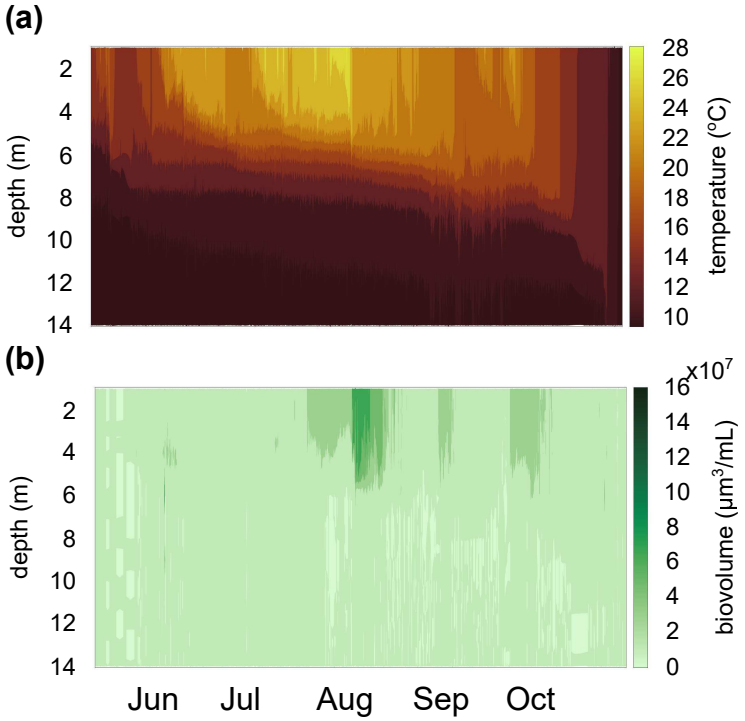

Figure 5: **(a)** Temperature contours and **(b)** biovolume contours at the location of the research station over the entire observation period. Air-water interface is at 0m.

(Fig. 6b) The seasonal trend of four important water column depths: the mixed layer depth (h_{ML}), the center of gravity of the DCL biovolume (z_{CG}), the thermocline depth (h_T), and the euphotic depth (h_{EP}) are depicted in Fig. 6c. The euphotic depth was essentially always well below the thermocline depth. The relative magnitude of the peak DCL biovolume concentration increases for a significant period of time in early June and early July (Fig. 6d). The data demonstrate that a deep cyanobacteria layer is associated with low wind speeds and air temperatures warmer than surface water temperatures. Both subsurface peaks eventually disperse, and do not form surface blooms.

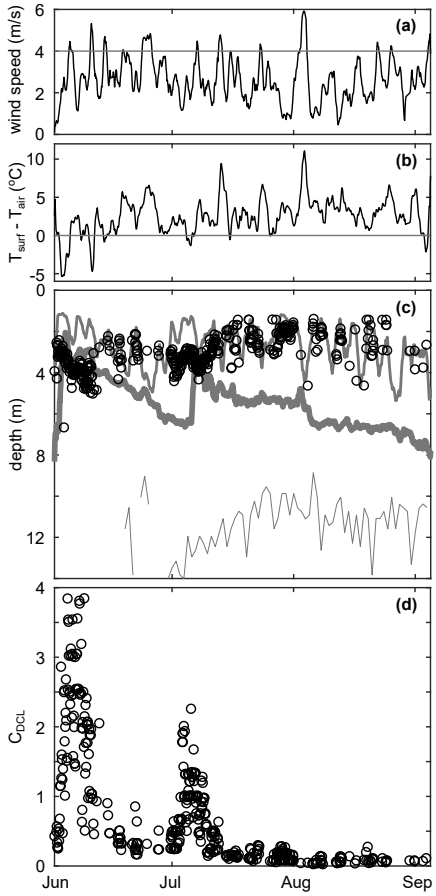

Figure 6: Time series of **(a)** wind speed (thin horizontal grey line indicates wind speed of 4 m/s), **(b)** T_{surf} - T_{air} (thin horizontal grey line indicates a temperature difference of zero), **(c)** important depth (mixed layer depth as the medium thickness grey line, thermocline depth as the thick grey line, euphotic depth as the thin grey line, and center of gravity of the DCL–as calculated by Eqn. 1–as the open black circles), and **(d)** relative peak magnitude of the DCL biovolume. There are two periods with significantly large C_{DCL} values: June 1st – June 13th and July 1st - July 9th. Air-water interface is at 0 m. Data was smoothed over a 24-hour window in order to clearly show long-term trends, with the exception of z_{CG} and C_{DCL}, which were left as calculated.

Comparing biovolume concentration profiles to temperature profiles seems to suggest a relationship between the stability of the thermal structure and vertical heterogeneity of the vertical biovolume distribution (Fig. 7). Profiles with a well-defined and deep uniform surface layer and metalimnion are associated with biovolume profiles with all the biomass concentrated in a uniform surface layer (Fig. 7a and 7b). Thermal profiles with a well-defined and shallow uniform surface layer but a terraced metalimnion are associated with biovolume profiles with deep cyanobacteria layers (Fig. 7c and 7d). Lastly, thermal profiles with a not well-defined surface layer are associated with biovolume profiles with surface (or near-surface) peaks (Fig. 7e and 7f). Eqns. 1 and 2 appear to appropriately characterize cyanobacterial vertical heterogeneity (see Appendix Appendix A for further discussion).

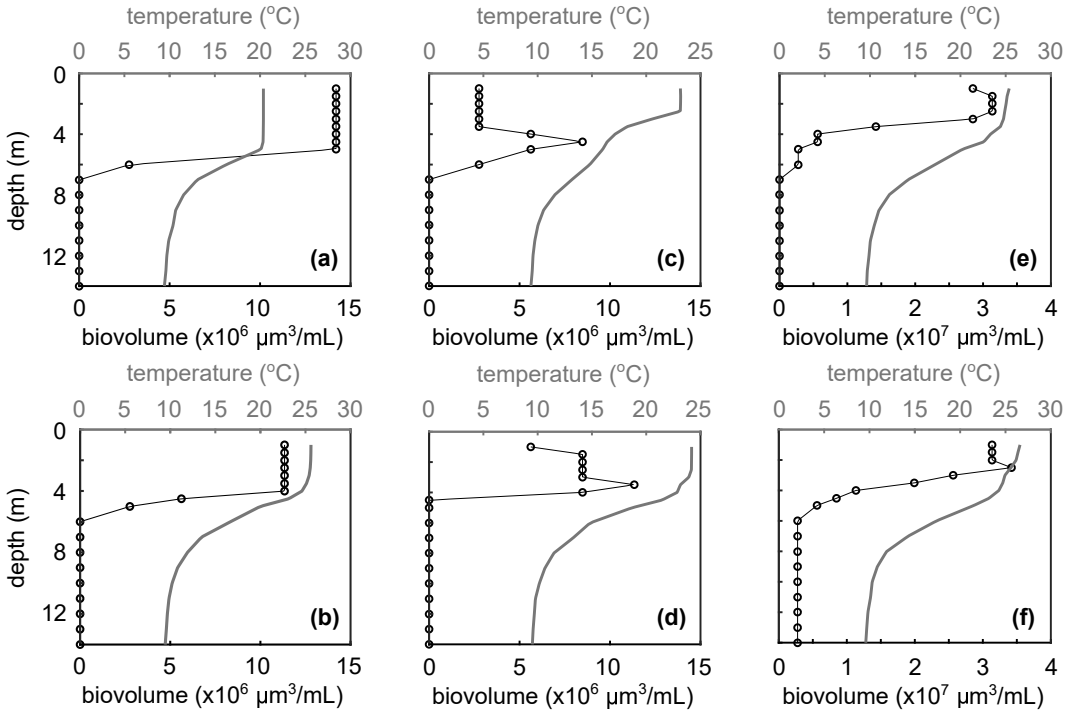

Figure 7: Example profiles taken **(a)** June 30, 2017 08:00, **(b)** July 13, 2017 02:00, **(c)** June 9, 2017 06:00, **(d)** June 17, 2017 20:00, **(e)** July 21, 2017 16:00, and **(f)** July 30, 2017 20:00. Thin black lines with open circle markers indicate biovolume concentration (bottom axis) and solid gray lines indicate temperature (top axis). **(a)** and **(b)** are examples of profiles with a uniform biovolume profile, **(c)** and **(d)** are examples of profiles with a deep cyanobacteria layer, and **(e)** and **(f)** are examples of profiles with a near-surface biovolume peak.

3.2 DCL Modeling results

Since nutrient conditions did not appear to be a significant driver of cyanobacterial vertical heterogeneity throughout the observation period of South Center Lake (Appendix Appendix B), the protocol outlined in Sec. 2.5 was used to fit models to C_{DCL} and z_{CG} (Table 2). The euphotic depth was deeper than the DCL for most of the observation period, so there was an insignificant difference between daytime and nighttime biovolume profile behavior, and only results for all profiles are shown.

Table 2: Stepwise regression results

DCL variable	parameter	coefficient estimate
a) z_{CG}, all profiles		
n = 417, r^2 = 0.66, RMSE = 0.034 (0.099 $\leq z_{CG} \leq$ 0.48)		
	intercept	-0.23
	$\tilde{h}_{ML}$	0.21
	$\tilde{h}_T$	0.71
	$\tilde{T}_{ML}$	110
	$\tilde{T}_T$	65
	$\tilde{h}_{ML}\tilde{h}_T$	1.0
	$\tilde{h}_T\tilde{T}_{ML}$	-190
	$\tilde{h}_T\tilde{T}_T$	-77
	$\tilde{T}_{ML}\tilde{T}_T$	-12000
b) C_{DCL}, all profiles		
n = 417, r^2 = 0.65, RMSE = 0.52 (0.027 $\leq C_{DCL} \leq$ 3.8)		
	intercept	0.33
	$\tilde{h}_T$	0.90
	$\tilde{T}_{ML}$	1300
	$\tilde{T}_T$	-970
	$\tilde{m}_T$	-190
	$\tilde{h}_T\tilde{T}_{ML}$	-2000
	$\tilde{T}_{ML}\tilde{m}_T$	44000
	$\tilde{T}_T\tilde{m}_T$	-18000

Stepwise regression results for **(a)** the center of gravity of the DCL biovolume and **(b)** the relative peak magnitude of the DCL biovolume. Full regression parameters listed in Table 1, although euphotic depth parameters were excluded since the euphotic depth was well below the thermocline for much of the observation period. The coefficient estimate column gives estimates of coefficients, and bolded p-values are those under the threshold of 0.05.

While the models outlined in Table 2 can predict values of C_{DCL} and z_{CG} to a relatively high degree, the models are rather cumbersome and difficult to assign physical meaning to. In an effort to achieve conceptually sound models that retain statistical significance, parsimonious models were generated using the full stepwise regression results as a first iteration and observational data as guides. Upon inspection of Fig. 6c and 6d, the difference in peak magnitude between the June and July peaky periods could be due to the difference in thermocline depth: a deeper thermocline depth in July seems to have led to a lower magnitude relative peak. Further, location of the DCL center of gravity seems to be related to the mixed layer depth (see also Fig. 7). Using these observations, input parameters from Tables 1 and 2 were stripped to just $\tilde{h}_T$ and $\tilde{T}_T$ for predicting C_{DCL} and $\tilde{h}_{ML}$ and $\tilde{T}_{ML}$ for predicting z_{CG}. These reduced complexity inputs generated the following expressions:

$$z_{CG} = 0.27 + 0.61\tilde{h}_{ML} - 22\tilde{T}_{ML} \tag{5}$$

which explains the data (n = 417 profiles) with an r^2 of 0.42 and a root-mean-squared error (RMSE) of 0.044. Eqn. 4 reduces to

$$C_{DCL} = 5.6 - 8.2\tilde{h}_T - 530\tilde{T}_T \tag{6}$$

which explains the data (n = 417 profiles) with an r^2 value of 0.57 and an RMSE of 0.57. These parsimonious models reduce input parameters to two while maintaining a large portion of the statistical significance (Fig. 8).

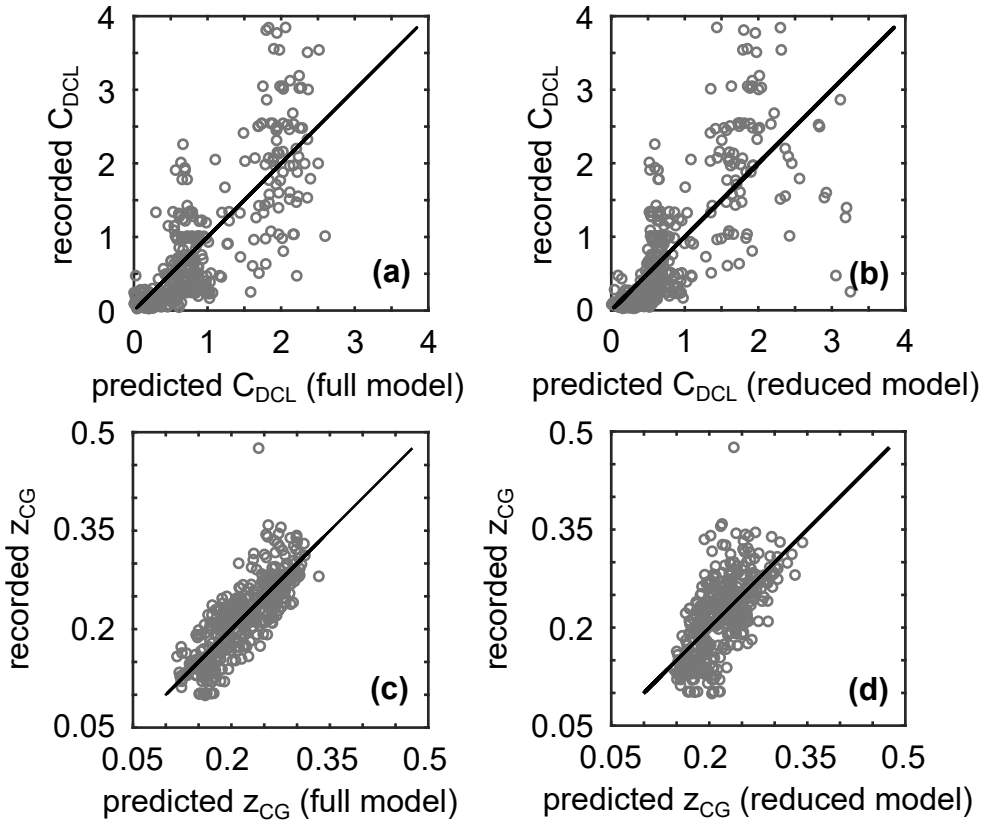

Figure 8: Goodness-of-fit results for models of **(a)** C_{DCL} using full stepwise regression results in Table 2b, (n = 417, r^2 = 0.65, RMSE = 0.52), **(b)** C_{DCL} using the simplified Eqn. 6 (n = 417, r^2 = 0.57, RMSE = 0.57), **(c)** z_{CG} using full stepwise regression results in Table 2a (n = 417, r^2 = 0.66, RMSE = 0.034), and **(d)** z_{CG} using the simplified Eqn. 5 (n = 417, r^2 = 0.42, RMSE = 0.044). Solid black lines show a one-to-one line.

4 Discussion

4.1 DCL behavior

Stepwise regression results indicate the center of gravity of the DCL biovolume is controlled by mixed layer depth and temperature (Eqn. 5), whereas the magnitude of the DCL biovolume peak is controlled by thermocline depth and temperature (Eqn. 6). Because *Microcystis* moves up and down a water column by adjusting cell density, we expect the thermocline depth–the depth of the largest magnitude density gradient–to act as a boundary condition. Not necessarily impenetrable (see early June period in Fig. 6c where the center of gravity of the DCL is actually below the thermocline depth), but more like a discontinuous step change from high to low diffusivity. Therefore, as the thermocline deepens, the width of habitable space for the algae increases. In this situation, we would expect the algae to diffuse throughout the entire habitable space, thereby decreasing peakiness. Following similar logic, increasing the temperature at the thermocline depth would also increase this habitable space, since temperature is monotonically decreasing and algae like it hot (Paerl

& Huisman, 2008), so we would again expect a more diffuse and less peaky distribution of algae.

Next, since well-mixed conditions will likely impede algal aggregation, we expect the center of gravity to deepen as the mixed layer depth deepens. Conversely, as a result of thermotaxis towards a preferred high temperature (water temperatures at the mixed layer never reached lethal conditions, as can be seen in Fig. 5a), we would expect the center of gravity to move shallower as the temperature at the mixed layer increases. This can be thought of as a balance between hydrodynamic forcings and biological preferences.

Eqns. 5 and 6 predict recorded values of C_{DCL} and z_{CG} to a reasonable accuracy with statistical significance for all profiles (Fig. 8). Given a temperature profile, Eqns. 5 and 6 will output DCL relative peak magnitude and center of gravity. Lakes are complex ecosystems, and cyanobacteria are remarkably sensitive to all different kinds of forcings, hydrodynamic and biological alike. However, it seems that a significant portion of the hydrodynamic dependencies can be packaged into thermal structure parameters that are relatively easy to measure. Further, in the stratified and eutrophic conditions seen throughout the observation period, biological forcings, which are difficult and time-consuming to measure, are secondary controls of the vertical distrubtion of cyanobacterial biomass.

It's prudent to note that these modeling results only make sense for the range of input variables given. For example, if the temperature in the mixed layer ever got too hot to be lethal to algae, any increase in temperature would likely lead to algae moving to cooler temperatures at deeper depths in the water column, and the DCL center of gravity would increase. However, the hottest water temperatures recorded at South Center Lake over the summer of 2017 was approximately 28^oC, which is right around the ideal temperature for *Microcystis*. Further, if the euphotic depth had not been below the thermocline for almost the entirety of the observation period, it is likely the euphotic depth would have had a statistically significant relationship with both C_{DCL} and z_{CG}. Lastly, nutrient conditions were favorable for *Microcystis* throughout the duration of the observation period (Appendix Appendix B). If the algae had to search for appropriate nutrient levels, this could negatively impact the accuracy of predictions.

4.2 DCL formation

Observational data suggest deep cyanobacteria layers are formed during periods of little to no wind shearing and natural convection (Fig. 6a and 6b). Results suggest that the location of the DCL center of gravity is determined by the mixed layer depth and the temperature at the mixed layer depth. To determine the role of wind shearing and natural convection, the penetrative convective velocity is introduced as

$$w_* = (Bh_{ML})^{\frac{1}{3}} \tag{7}$$

where B is the buoyancy flux in m^2/s^3 (Imberger, 1985). If we assume the air-water temperature difference is the dominant heat flux term, we can define the buoyancy flux at the water surface as

$$\begin{aligned} B &= \frac{g\alpha}{\rho C_P} H_Q \\ &\approx \frac{g\alpha}{\rho C_P}\left(k\frac{\partial T}{\partial z}\right)_{z=0} \\ &\approx \frac{g\alpha}{\rho C_P}\left(k\frac{T_{surf}-T_{air}}{\delta_t}\right) \end{aligned} \tag{8}$$

where g is the gravitational acceleration (m/s^2), α is the coefficient of thermal expansion (1/K), ρ is the water density (kg/m^3), C_P is the specific heat of water (J/kg/K), H_Q is the total heat flux at the water surface (W/m^2), k is the thermal conductivity of water

(W/m/K), and taking $T_{surf} \approx T_{ML}$ by assuming an infinitely small air-side boundary layer. A positive buoyancy flux, then, indicates the lake is undergoing surface cooling. J. Wu (1971) provides an estimation for δ_t, the thermal diffusivity layer thickness (m), to be

$$\delta_t = 5.5\frac{\nu}{u_*} \tag{9}$$

where ν is the kinematic viscosity of water (m^2/s) and u_* is the shear velocity at the water surface (m/s). We can now introduce a Reynolds number for penetrative convection at the water surface to be

$$Re = \frac{w_* h_{ML}}{\nu}$$

$$= \frac{(Bh_{ML})^{\frac{1}{3}} h_{ML}}{\nu}$$

Hence,

$$Re = \frac{\left(g\alpha D_T (T_{ML} - T_{surf})\right)^{\frac{1}{3}} h_{ML}}{\nu} \tag{10}$$

where $D_T = \frac{k h_{ML}}{\rho C_P \delta_t}$ is the thermal dispersion coefficient. Using this formulation for a Reynolds number relevant to surface thermal cooling, profiles undergoing conditions such that Re > 5×10^4 virtually never formed a DCL for the entirety of the observation period (Fig. 9).

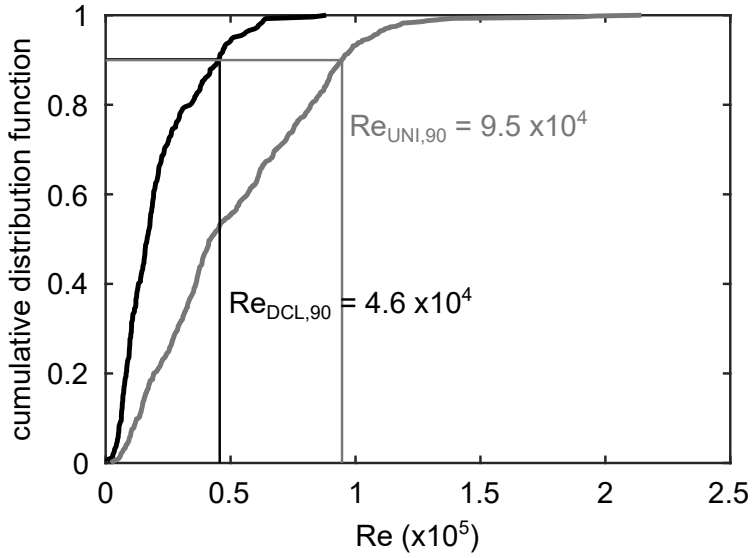

Figure 9: Surface thermal cooling Reynolds number cumulative distribution function (CDF). Black line is the CDF for profiles with a DCL, gray line is the CDF for profiles without a DCL. 90% of profiles with a DCL have concurrent Re values of 4.6×10^4 or less; 90% of profiles without a DCL have concurrent Re values of 9.5×10^4 or less.

Eqn. 10 states that Re $\sim h_{ML}(T_{surf} - T_{air})^{\frac{1}{3}}$. These results reveal two important points. The first is that the deeper the mixed layer depth, the less likely it is that a DCL will form (Fig. 10a and 10b). In fact, the two situations seem to have two entirely different distributions of mixed layer depths: profiles with a DCL follow a power law, whereas profiles wihtout a DCL follow a uniform distribution. Since the euphotic depth was well below the thermocline for the entirety of the observation period (Fig. 6c), light was not limiting the

aggregation of *Microcystis* below the mixed layer depth. The lack of a DCL, then, is likely due to the physical drivers, like wind shearing (Pollard et al., 1972; Ushijima & Yoshikawa, 2020), of a deepening mixed layer depth. Secondly, from Eqn. 10, we can also infer that the greater the surface water temperature is relative to the air temperature, the less likely it is that a DCL will form (Fig. 10c and 10d). The temperature difference ($T_{surf} > T_{air}$) promotes natural convection-induced turbulence at the water surface. In effect, the data indicate the likelihood of a DCL occurring decreases as surface layer processes like wind shearing and natural convection increase.

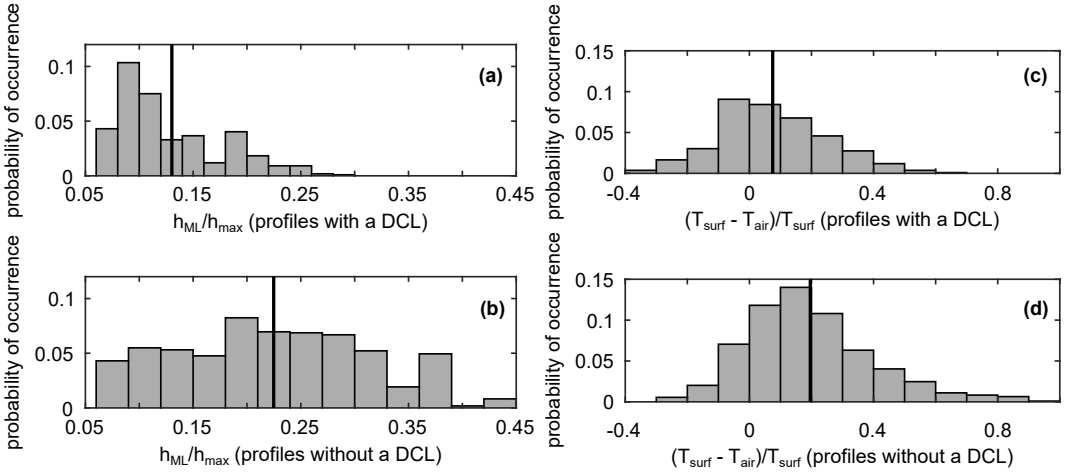

Figure 10: Histograms of **(a)** normalized mixed layer depth for profiles with a DCL, **(b)** normalized mixed layer depth for profiles without a DCL, **(c)** normalized air-water temperature difference for profiles with a DCL, and **(d)** normalized air-water temperature difference for profiles without a DCL. Vertical lines indicate mean values of **(a)** 0.13, **(b)** 0.22, **(c)** 0.076, and **(d)** 0.19.

4.3 DCL fate

After formation and behavior of the deep cyanobacteria layer comes its fate: Does it disperse and form a uniform algae profile, or does it form a surface bloom? Both the June and July DCLs develop large peaks, although the June DCL center of gravity travels much deeper than the July. Water temperatures in the surface layer are high enough to sustain cyanobacterial life, nutrient conditions are sufficient, and yet neither subsurface peaks form a surface bloom. To address this, we introduce a new term, ζ defined as

$$\zeta = \frac{z_{CG}}{\frac{1}{h_{max}} \frac{\int_0^{h_{max}} zCdz}{\int_0^{h_{max}} Cdz}} \tag{11}$$

Eqn. 11 is a ratio of the center of gravity of the DCL to the center of gravity of the whole profile. This will give a measure of the abnormality of the DCL peak. For example, if the entire biovolume profile followed a Gaussian distribution, then the center of gravity of the DCL would equal the center of gravity of the whole profile, and $\zeta = 1$. This would also be true if biovolume concentrations were zero everywhere except the DCL. However, if there is significant biovolume in the mixed layer, then this would shift the center of gravity of the whole profile shallower, relative to the center of gravity of just the DCL, resulting in $\zeta > 1$. Similarly, ζ will be less than one if the DCL fails to capture all of the biovolume below the mixed layer.

It was determined that, although the values of z_{CG} were significantly different for the June and July peaky period, the ζ values of each were approximately the same, $\zeta = 1$. Further, there appears to be a sinusoidal seasonal trend in ζ that could indicate when a bloom will occur (thick black line in Fig. 11). The bloom occurs at $\zeta = 0.64$, according to the fitted sine curve; this is also the value of ζ when averaged over the three days immediately preceding the bloom (thin black vertical line demarcates when the bloom took place, thin black horizontal line shows the prior three days averaged value of ζ). To check this trend, 2018 data from Ramsey Lake–a deep, dimictic, and eutrophic lake with a history of *Microcystis* blooms–was investigated. For profiles taken when the euphotic depth was deeper than the thermocline depth, we see a similar trend, with algal blooms occurring when ζ values dip below the approximate 0.6 threshold.

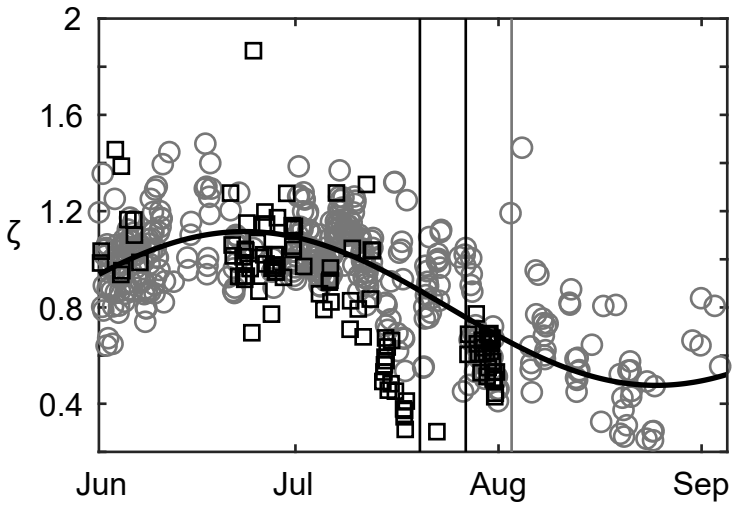

Figure 11: Seasonal trend of ζ from South Center Lake in 2017 (open gray circles) and Ramsey Lake in 2018 (open black squares). Thick black line indicates the best fit periodic function to South Lake determined to be $\zeta = 0.80 + 0.32\sin(0.05t + 7 \times 10^5)$, where t here is the Matlab serial date number ($r^2 = 0.56$, p-value = $3.2{\times}10^{-75}$). Thin black vertical lines indicate dates of harmful algal blooms in Ramsey Lake (July 20th and 27th, 2018), and thin gray vertical line is the date of the harmful algal bloom in South Center Lake (August 3rd, 2017).

To further explore this, we consult individual profiles for $\zeta < 1$, $\zeta = 1$, and $\zeta > 1$ (Fig. 12). When $\zeta = 1$ (Fig. 12a), as is the case for the peaky periods in June and July, we see low biovolume concentrations in the mixed layer and below the DCL. In these situations, integrating biovolume over the entire water column is essentially the same as integrating biovolume just within the DCL, hence the center of gravity of the whole profile aligns with the center of gravity of just the DCL. When $\zeta > 1$ (Fig. 12b), as is the case in between the two peaky periods in June and July, we see large concentrations of biovolume within the mixed layer relative to the biovolume concentration in the DCL. This brings the center of gravity of the whole profile shallower, when compared to the center of gravity of just the DCL. When $\zeta < 1$ (Fig. 12c), as is the case just before the surface bloom, we see a narrow DCL but a wide distance between the mixed layer depth and the thermocline depth. Using the same logic that informed our model in the previous section, a deep thermocline gives algae a larger habitable space. So even though the DCL itself occupies a narrow band immediately below the mixed layer, not insignificant populations of algae are capable of living below the DCL, thusly moving the center of gravity of the whole profile deeper compared to the center of gravity of just the DCL.

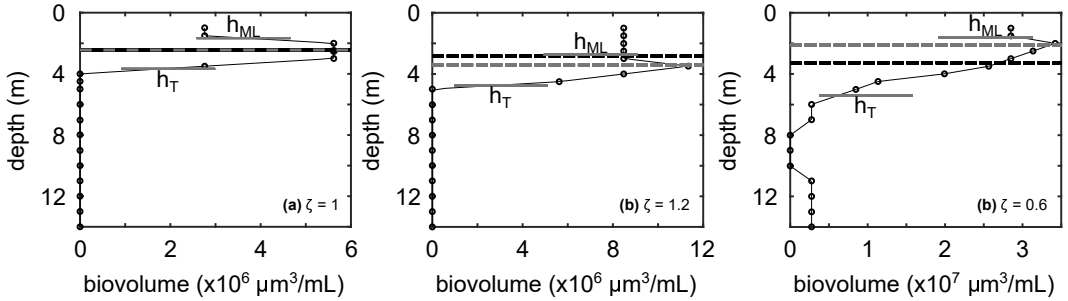

Figure 12: Examples of profiles for **(a)** $\zeta = 1$, profile taken July 1 2017 04:00, **(b)** $\zeta > 1$, profile taken June 21 2017 02:00, and **(c)** $\zeta < 1$, profile taken at July 31 2017 12:00. Black dashed lines indicate center of gravity of the whole biovolume profile, and gray dashed lines indicate center of gravity of the DCL.

Conceptually, profiles with $\zeta < 1$ appear to have a much easier journey from DCL to surface HAB compared to profiles with $\zeta \geq 1$. Recall also the phenomenon of bioconvection, in which the motion of dense algae introduces hydrodynamic instabilities into the water column (Sommer et al., 2017; Sepúlveda Steiner et al., 2019). Profiles with $\zeta \geq 1$ appear more likely to induce hydrodynamic instabilities, potentially changing the thermal structure of the lake, and inhibiting surface bloom formation.

The aim of this analysis is not to be conclusive, but rather provocative, in the hopes of fueling further thought and research. The center of gravity parameter is new to the field of DCL research, but its usefulness appears hopeful. If the shape of the DCL biovolume relative to the shape of the entire biovolume profile does, in fact, exhibit a predictable seasonal trend, as is suggested in Fig. 11, then this could be a missing link between predicting vertical distribution of algae and predicting harmful algal bloom formation.

5 Conclusions

A high-frequency, long-duration research station was anchored in a eutrophic and dimictic lake for the entirety of summer stratification. This research station recorded meteorological measurements every five minutes and water quality profiles every two hours. Two key parameters were introduced to describe cyanobacterial vertical heterogeneity: C_{DCL}, a measure of the relative peak biovolume concentration magnitude, and z_{CG}, the center of gravity of the biovolume concentration with the deep cyanobacteria layer (DCL). A stepwise regression analysis was performed to determine the dependence of these two variables on abiotic parameters of the lake.

A DCL was present for a large portion of the majority of the summer season. Results indicate the magnitude of the DCL peak depends on physical conditions at the thermocline, but the center of gravity of the DCL depends on physical conditions at the mixed layer. It was also shown that a large Reynolds number related to surface cooling, $\mathrm{Re} > 5{\times}10^4$, inhibits the formation of a DCL.

Although definitions differed slightly, the findings presented in this paper corroborate the findings of Scofield et al. (2017) at Lake Ontario: thermal structure parameters can explain significant variability of where in the water column a DCL forms and how large the peak magnitude of the DCL gets. The machine learning algorithm developed by Xu et al. (2019) to determine key parameters and patterns of thermal and biological vertical profiles could be used to systemically determine C_{DCL} and z_{CG} from field data, in order to provide more consistent protocol and definitions between studies. This would expedite

research, allowing for these parameters to be modeled in a large number of lakes with different light, temperature, and nutrient regimes. The models and parameters presented in this paper not only provide phenomenological insight towards *Microcystis* lifestyles, but their utilitarian simplicity in both form and ease of measurement will also help lake water systems stakeholders with limited funds and manpower appropriately manage their resources.

Appendix A Vertical heterogeneity and the DCL

To ensure DCL definitions are physically meaningful and do not obscure biovolume vertical heterogeneities within the mixed layer, we introduce

$$C_{ML} = \frac{C_{ML,max} - C_{ML,avg}}{C_{ML,avg}} \tag{A1}$$

Eqn. A1 gives the magnitude of the biovolume concentration peak within the mixed layer relative to the average concentration in the mixed layer. Our assumption is that biovolume vertical heterogeneities can only occur below the mixed layer, because mixing processes within the mixed layer will dominate any depth-specific growth or migration of cyanobacteria, thusly wiping out any possible biovolume aggregation. Values of C_{ML} close to zero will validate this assumption.

Results indicate an average value of $C_{ML,avg} = 0.058$, which is much lower than the average value of C_{DCL}, $C_{DCL,avg} = 0.79$ (Fig. A1). Further, there appears to be no significant difference in the distribution of C_{ML} between profiles with and without a DCL. Meaning the existence of a DCL does not impact the biovolume heterogeneity, or lack thereof, within the mixed layer. For these reasons, the authors suggest that the definition of a DCL, its bounds, and its parameters detailed in Section 2.4 accurately describe biovolume vertical heterogeneities.

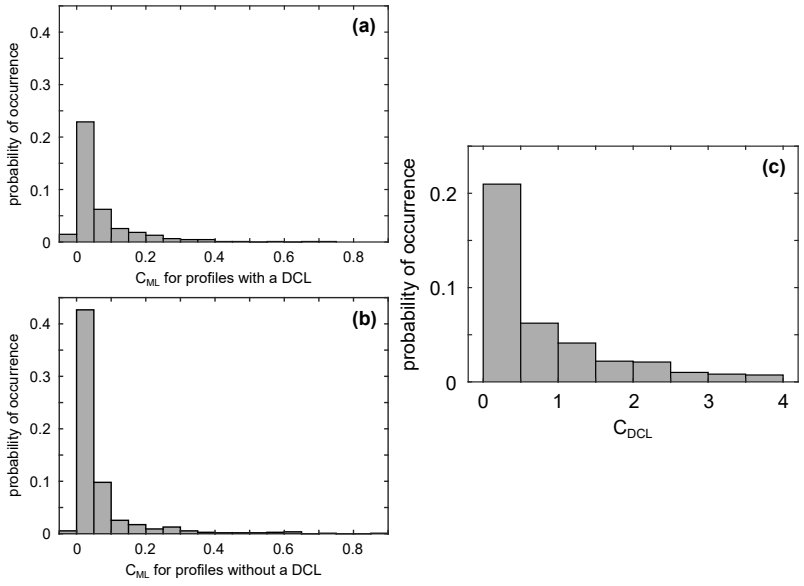

Figure A1: Histograms of **(a)** C_{ML} for profiles with a DCL, **(b)** C_{ML} for profiles without a DCL, and **(c)** C_{DCL}. There appears to be no discernible difference in C_{ML} distribution between profiles with and without a DCL. The largest value C_{ML} takes for all profiles is about 0.9, or a 90% increase in peak value from the mean value. This is much lower than the largest value of C_{DCL}, which is around 4.

Appendix B Nutrients

Nutrient grab samples were taken on an approximately weekly basis to quantify nitrate (NO_3^-) and phosphate (PO_4^{3-}) concentrations. Nitrate concentrations were below the detection limit of 0.02 mg/L for all depths for the entire summer season, and phosphate concentrations at depths of 1m, 3m, 6m, and 10m are shown in Fig. B1. Even at the lowest recorded phosphate concentration of 0.02 mg/L, the highest N:P ratio was 1, indicating nitrogen was likely limiting *Microcystis* growth during the entire monitoring period (Wurtsbaugh et al., 2019). However, Marinho et al. (2007) demonstrated that although N:P ratios less than 14 are correlated with *Microcystis* dominance in the field, this is likely a result of *Microcystis* dominance and not a cause (Fujimoto et al., 1997). Surface level concentrations of phosphate (1m data) remain consistently low until mid-September, well after the surface bloom of early August had formed and dissipated. The highest concentrations of phosphate occur in mid-July, after the July subsurface peaky period but before the August surface bloom. The phosphate profile changed from relatively uniform to almost monotonically increasing with depth in a matter of a week during this same time. However, this change in shape of the phosphate profile led to no distinguishable change in the shape of the biovolume profile. For these reasons, we suggest that nutrients played a secondary role in the vertical heterogeneity of *Microcystis* in South Center Lake for the summer 2017 season. Namely, the nutrient conditions of South Center Lake allowed *Microcystis* to thrive, but did not control vertical distribution of cells.

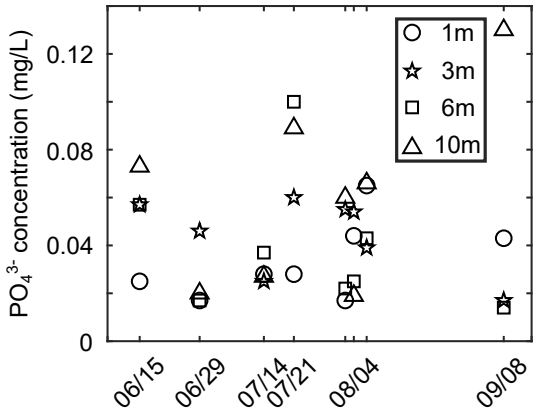

Figure B1: Phosphate concentrations (from grab samples) time series at location of research station. Circles indicate phosphate concentration at 1m, stars at 3m, squares at 6m, and triangles at 10m. Sampling dates shown on x axis.

Acknowledgments

Data archiving is underway at the Data Repository for University of Minnesota. Funding was provided by the Legislative-Citizen Commission on Minnesota Resources and the National Science Foundation Graduate Research Funding Program. The authors wish to thank the Minnesota Pollution Control Agency for their supplemental data provided that was used to validate research station and grab sample measurements. Finally, a special thank you goes out to Jiaqi You, for providing guidance and conducting lab analyses of grab samples; Dr. Shahram Missaghi, for help with outreach and coordination; and Dr. Anne Ahlvers-Wilkinson, for jump-starting the entire project.

References

Bormans, M., Sherman, B., & Webster, I. (1999). Is buoyancy regulation in cyanobacteria an adaptation to exploit separation of light and nutrients? *Marine and Freshwater Research*, *50*(8), 897–906.

Brooks, A. S., & Torke, B. G. (1977). Vertical and seasonal distribution of chlorophyll a in lake michigan. *Journal of the Fisheries Board of Canada*, *34*(12), 2280–2287.

Cao, H.-S., Kong, F.-X., Luo, L.-C., Shi, X.-L., Yang, Z., Zhang, X.-F., & Tao, Y. (2006). Effects of wind and wind-induced waves on vertical phytoplankton distribution and surface blooms of microcystis aeruginosa in lake taihu. *Journal of Freshwater Ecology*, *21*(2), 231–238.

Cullen, J. J. (1982). The deep chlorophyll maximum: comparing vertical profiles of chlorophyll a. *Canadian Journal of Fisheries and Aquatic Sciences*, *39*(5), 791–803.

Cullen, J. J. (2015). Subsurface chlorophyll maximum layers: enduring enigma or mystery solved?

Engel, L., Valley, R., & Vanderbosch, D. (2011). *Sentinel lake assessment report south center lake (13-0027) chisago county, minnesota* (Tech. Rep.). Minnesota Pollution Control Agency and Minnesota Department of Natural Resources.

Fogg, G., & Walsby, A. (1971). Buoyancy regulation and the growth of planktonic blue-green algae. *Internationale Vereinigung für Theoretische und Angewandte Limnologie: Mitteilungen*, *19*(1), 182–188.

Fujimoto, N., Sudo, R., Sugiura, N., & Inamori, Y. (1997). Nutrient-limited growth of microcystis aeruginosa and phormidium tenue and competition under various n: P supply ratios and temperatures. *Limnology and Oceanography*, *42*(2), 250–256.

Ganf, G., & Oliver, R. (1982). Vertical separation of light and available nutrients as a factor causing replacement of green algae by blue-green algae in the plankton of a stratified lake. *The Journal of Ecology*, 829–844.

Hozumi, A., Ostrovsky, I., Sukenik, A., & Gildor, H. (2019). Turbulence regulation of microcystis surface scum formation and dispersion during a cyanobacteria bloom event. *Inland Waters*, 1–20.

Huisman, J., Codd, G. A., Paerl, H. W., Ibelings, B. W., Verspagen, J. M., & Visser, P. M. (2018). Cyanobacterial blooms. *Nature Reviews Microbiology*, *16*(8), 471.

Huisman, J., Thi, N. N. P., Karl, D. M., & Sommeijer, B. (2006). Reduced mixing generates oscillations and chaos in the oceanic deep chlorophyll maximum. *Nature*, *439*(7074), 322.

Imberger, J. (1985). The diurnal mixed layer. *Limnology and oceanography*, *30*(4), 737–770.

Liu, M., Ma, J., Kang, L., Wei, Y., He, Q., Hu, X., & Li, H. (2019). Strong turbulence benefits toxic and colonial cyanobacteria in water: A potential way of climate change impact on the expansion of harmful algal blooms. *Science of The Total Environment*.

Marinho, M. M., et al. (2007). Influence of n/p ratio on competitive abilities for nitrogen and phosphorus by microcystis aeruginosa and aulacoseira distans. *Aquatic Ecology*, *41*(4), 525–533.

Marti, C. L., Imberger, J., Garibaldi, L., & Leoni, B. (2016). Using time scales to characterize phytoplankton assemblages in a deep subalpine lake during the thermal stratification period: L ake i seo, i taly. *Water Resources Research*, *52*(3), 1762–1780.

Medrano, E. A., Uittenbogaard, R., Pires, L. D., Van De Wiel, B., & Clercx, H. (2013). Coupling hydrodynamics and buoyancy regulation in microcystis aeruginosa for its vertical distribution in lakes. *Ecological Modelling*, *248*, 41–56.

O'Neil, J., Davis, T., Burford, M., & Gobler, C. (2012). The rise of harmful cyanobacteria blooms: the potential roles of eutrophication and climate change. *Harmful algae*, *14*, 313–334.

Paerl, H. W., & Huisman, J. (2008). Blooms like it hot. *Science*, *320*(5872), 57–58.

Pollard, R. T., Rhines, P. B., & Thompson, R. O. (1972). The deepening of the wind-mixed layer. *Geophysical & Astrophysical Fluid Dynamics*, *4*(1), 381–404.

Read, J. S., Hamilton, D. P., Jones, I. D., Muraoka, K., Winslow, L. A., Kroiss, R., ... Gaiser, E. (2011). Derivation of lake mixing and stratification indices from high-

resolution lake buoy data. *Environmental Modelling & Software*, *26*(11), 1325–1336.

Reynolds, C. S., Oliver, R. L., & Walsby, A. E. (1987). Cyanobacterial dominance: the role of buoyancy regulation in dynamic lake environments. *New Zealand journal of marine and freshwater research*, *21*(3), 379–390.

Sanful, P. O., Otu, M. K., Kling, H., & Hecky, R. E. (2017). Occurrence and seasonal dynamics of metalimnetic deep chlorophyll maximum (dcm) in a stratified meromictic tropical lake and its implications for zooplankton community distribution. *International Review of Hydrobiology*, *102*(5-6), 135–150.

Scofield, A. E., Watkins, J. M., Weidel, B. C., Luckey, F. J., & Rudstam, L. G. (2017). The deep chlorophyll layer in lake ontario: extent, mechanisms of formation, and abiotic predictors. *Journal of Great Lakes Research*, *43*(5), 782–794.

Sepúlveda Steiner, O., Bouffard, D., & Wüest, A. (2019). Convection-diffusion competition within mixed layers of stratified natural waters. *Geophysical Research Letters*, *46*(22), 13199–13208.

Somavilla, R., Rodriguez, C., Lavín, A., Viloria, A., Marcos, E., & Cano, D. (2019). Atmospheric control of deep chlorophyll maximum development. *Geosciences*, *9*(4), 178.

Sommer, T., Danza, F., Berg, J., Sengupta, A., Constantinescu, G., Tokyay, T., ... others (2017). Bacteria-induced mixing in natural waters. *Geophysical Research Letters*, *44*(18), 9424–9432.

Thomas, R., & Walsby, A. (1985). Buoyancy regulation in a strain of microcystis. *Microbiology*, *131*(4), 799–809.

Thomas, R., & Walsby, A. (1986). The effect of temperature on recovery of buoyancy by microcystis. *Microbiology*, *132*(6), 1665–1672.

Ushijima, Y., & Yoshikawa, Y. (2020). Mixed layer deepening due to wind-induced shear-driven turbulence and scaling of the deepening rate in the stratified ocean. *Ocean Dynamics*, 1–8.

Wallace, B. B., Bailey, M. C., & Hamilton, D. P. (2000). Simulation of vertical position of buoyancy regulating microcystis aeruginosa in a shallow eutrophic lake. *Aquatic Sciences*, *62*(4), 320–333.

Wilkinson, A., Hondzo, M., & Guala, M. (2020). Vertical heterogeneities of cyanobacteria and microcystin concentrations in lakes using a seasonal in situ monitoring station. *Global Ecology and Conservation*, *21*, e00838.

Woolway, R. I., Jones, I. D., Hamilton, D. P., Maberly, S. C., Muraoka, K., Read, J. S., ... Winslow, L. A. (2015). Automated calculation of surface energy fluxes with high-frequency lake buoy data. *Environmental Modelling & Software*, *70*, 191–198.

Wu, J. (1971). An estimation of oceanic thermal-sublayer thickness. *Journal of Physical Oceanography*, *1*(4), 284–286.

Wu, X., Noss, C., Liu, L., & Lorke, A. (2019). Effects of small-scale turbulence at the air-water interface on microcystis surface scum formation. *Water Research*, *167*, 115091.

Wurtsbaugh, W. A., Paerl, H. W., & Dodds, W. K. (2019). Nutrients, eutrophication and harmful algal blooms along the freshwater to marine continuum. *Wiley Interdisciplinary Reviews: Water*, *6*(5).

Xiao, M., Li, M., & Reynolds, C. S. (2018). Colony formation in the cyanobacterium microcystis. *Biological Reviews*, *93*(3), 1399–1420.

Xu, W., Collingsworth, P. D., & Minsker, B. (2019). Algorithmic characterization of lake stratification and deep chlorophyll layers from depth profiling water quality data. *Water Resources Research*.

Yao, B., Liu, Q., Gao, Y., & Cao, Z. (2017). Characterizing vertical migration of microcystis aeruginosa and conditions for algal bloom development based on a light-driven migration model. *Ecological research*, *32*(6), 961–969.

Zhu, W., Feng, G., Chen, H., Wang, R., Tan, Y., & Zhao, H. (2018). Modelling the vertical migration of different-sized microcystis colonies: coupling turbulent mixing and buoyancy regulation. *Environmental Science and Pollution Research*, *25*(30), 30339–30347.